Charge Relaxation and Gain Depletion for Candidate Secondary Electron Emission Materials

Zeke Insepov, Valentin Ivanov, Jeffrey Elam, Bernhard Adams

Abstract – **Microchannel plates (MCPs) are widely used in photodetectors with a picosecond resolution. Two main characteristics of MCPs, gain and timing resolution, strongly depend on the materials parameters, as well as on the history of electron avalanche evolution. The most important effect that can significantly change the efficiency of an MCP is the effect of saturation of the electronic current, which occurs at high-level input signals. In this paper, the saturation effects are studied numerically, as they are applicable to analysis of large-area, fast photodetectors. It is shown that the saturation effect for short pulses can be reduced by introducing a thin, resistive layer between the bulk material and the emissive coating. The gain and time resolution dependencies on the pore size and voltage are studied numerically. The results are compared with the simulations of other authors and available experimental data.**

I. Introduction

Measurements in particle and accelerator physics are limited by the time resolution of the devices with which the individual particles are detected. These measurements include particle identification through time of flight in major experiments such as CDF at Fermilab and Atlas and CMS at the Large Hadron Collider, as well as experiments in accelerator physics.

A large-area photodetector consists of a photo cathode, which accepts photons from a Cherenkov counter or other photon source; a multichannel plate (MCP); an anode; and an accelerating gap between these parts. The MCP produces cascades of secondary electrons captured by the anode electronic circuit.

II. Computation of Charge Relaxation Time

The electrophysical properties of secondary-emissive films can be modified significantly by adjusting the relative proportions of the elemental composition in the materials. This strategy has been used to control film properties such as refractive index, dielectric constant, lattice constant, hardness, charge storage capacity, and surface roughness [1]. Atomic layer deposition (ALD) is a promising technique for emissive film fabrication. ALD methods also have been used to deposit compound films including nanostructured films, oxides, and conductive materials. The ZnO/Al_2O_3 alloy films for this study were prepared by using an ALD technique. By adjusting the ALD pulse sequence, the ZnO/Al_2O_3 alloy film composition was varied from 0% to 100% ZnO [1]. ZnO/Al_2O_3 alloy films may provide a low-cost alternative to indium tin oxide as a transparent conducting material for flat-panel displays and solar cells.

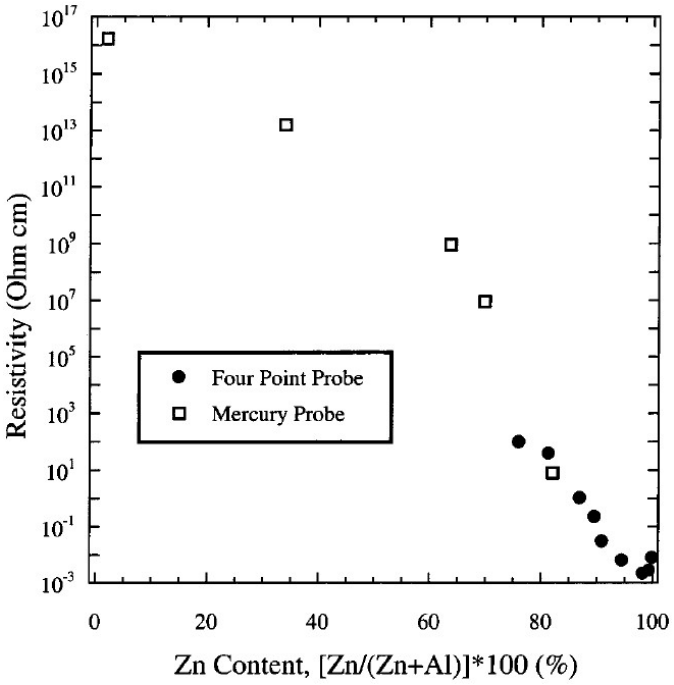

Fig. 1. Resistivity of ZnO/Al_2O_3 alloy films used in this work [1].

Figure 1 shows the resistivity of the ZnO/Al_2O_3 alloy films used in this work and calculated as follows:

$$\rho = R\frac{S}{l} = (90-500)\times 10^{12}\,\Omega\frac{1.29\times 10^{-9}\,m^2}{1.6\times 10^{-3}\,m^2},$$
$$\rho = (0.725-4.03)\times 10^{10}\,(\Omega\cdot cm), \quad (1)$$
$$\sigma = (1.38-0.25)\times 10^{-10}\,(\Omega\cdot cm)^{-1}.$$

Here ρ and σ are the resistivity and conductivity of the compound films, respectively. Based on these constraints, the composition of the films was chosen as follows: 40% Al_2O_3 and 60% of ZnO. The relaxation time can be roughly estimated as a charge relaxation (Maxwell) time [2]:

$$\tau_M = \varepsilon\varepsilon_0/\sigma, \quad (2)$$

which gives 6.1×10^{-3} seconds.

Manuscript submitted November 13, 2010.

Z. Insepov is with Argonne National Laboratory, Argonne, IL 60439, USA (telephone: 630-252-5049, e-mail: insepov@anl.gov).

V. Ivanov was with Muons Inc., Batavia, IL 60610, USA. (telephone: 408-568-1483, e-mail: vivanov@fnal.gov).

J. Elam is with Argonne National Laboratory, Argonne, IL 60439, USA (e-mail: jelam@anl.gov).

B. Adams is with Argonne National Laboratory, Argonne, IL 60439, USA (e-mail: badams@anl.gov).

H. Frisch is with the University of Chicago, Chicago, IL 60637, USA (e-mail: frisch@hep.uchicago.edu)

Table 1. Dielectric constants [3] and resistivities of Al_2O_3/ZnO ALD films [1]

% DEZ* exposures	0	10	25	33	50
Dielectric constant	6.8	6.5	6.9	7.2	6.6
Resistivity (Ω cm)	$\sim 10^{16}$	5×10^{15}	5×10^{14}	1×10^{14}	1×10^{13}
Relaxation times, s	6×10^{3}	2.9×10^{3}	305	64	5.8

Table 2. Properties of the bulk material (borosilicate glass)

Bulk Material	Borosilicate glass
Dielectric constant	5.8
Conductivity, S/m	1×10^{-17}
Relaxation time, s	5.1×10^{6}

The following pore structure was used: pore diameters 20 μm, thickness of Al_2O_3/ZnO coatings 1–5 μm, aspect ratio 40.

Figure 2 shows two different charge distribution geometries that were calculated with the equation set (3): (a) spherical and (b) cylindrical.

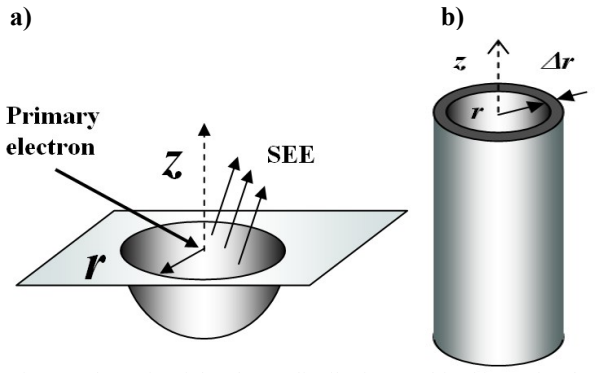

Fig. 2. Schematic of the charge distribution used in this work. The following parameters were used: (a) r = 10 nm and (b) r = 20 mm, Δr = 10 nm, aspect ratio 40.

Materials constants and physical properties of alloy films, such as surface roughness, resistivity, dielectric constants, and film thickness (see Tables 1 and 2) were obtained that were suitable for using these materials as resistive and emissive layers in large-area photodetecting MCPs, as compared to conventional glass substrates. Charge relaxation and gain depletion mechanisms, effects of a strong electric field, and geometry parameters of the coating for a large-area, fast photodetector were analyzed and discussed in Ref. [4].

A new ambipolar, solid-state, plasma drift-diffusion model of the charge relaxation in materials such as ZnO/Al_2O_3 in various combinations of the content was proposed that included generation of electrons and holes via impact ionization due to acceleration in a strong electric field [5]. Some of the equations of this model are given in equation (3) [2,6-8].

$$
\begin{aligned}
&\vec{J}_e = eD_e\nabla N_e + e\mu_e N_e\vec{E},\\
&\vec{J}_h = -eD_h\nabla N_h + e\mu_h N_h\vec{E},\\
&div\,\vec{E} = \rho/\varepsilon\varepsilon_0,\ \rho = N_h - N_e,\\
&\frac{\partial N_e}{\partial t} = \frac{1}{q}\nabla J_e = D_e\Delta N_e + eN_e\mu_e/\varepsilon\varepsilon_0(N_h - N_e) + G_{ii},\\
&\frac{\partial N_h}{\partial t} = -\frac{1}{q}\nabla J_h = D_h\Delta N_h - eN_h\mu_h/\varepsilon\varepsilon_0(N_h - N_e),\\
&\mu_{e,h} = \sigma_{e,h}/e\,N_{e,h},\ \ D_{e,h} = \mu_{e,h}k_BT/e.
\end{aligned}
\tag{3}
$$

Here e is the elemental charge amount (e > 0), $D_{e,h}$ are the diffusion coefficients, and $\mu_{e,h}$ are the mobility of electrons and holes at temperature T created by electron impacts and ionization in the space charge field, G_{ii}. The Einstein relationship between the diffusion coefficients and the mobility allows one to use the electric-field-dependent diffusion coefficients. $N_{e,h}$ are the corresponding carrier densities, and $J_{e,h}$ are the fluxes of carriers.

The following conductivity of an *AZO* film with 20% Al was used: μ=10^7 (Ω cm). The diffusion coefficients of amorphous alumina are unknown. Therefore, we found the diffusion coefficients of alumina via alumina carrier mobility that are given for some mixtures in Ref. [9]. Assuming linear dependence between conductivity and mobility, we extrapolate the mobility of a mixture Al_2O_3+ZnO from low to high aluminum content.

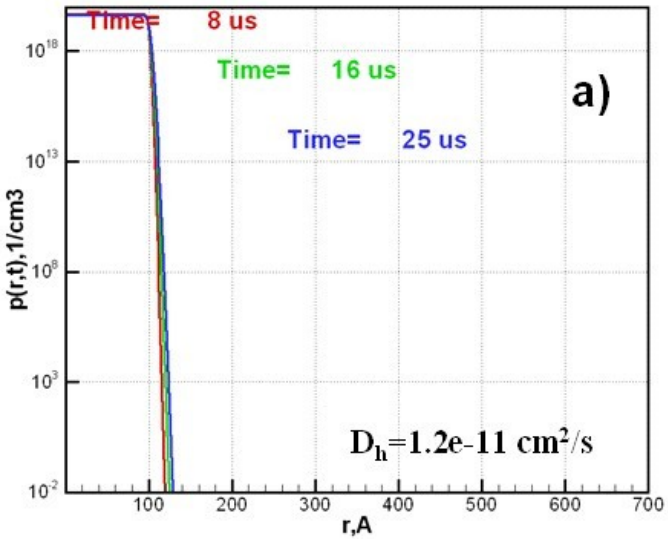

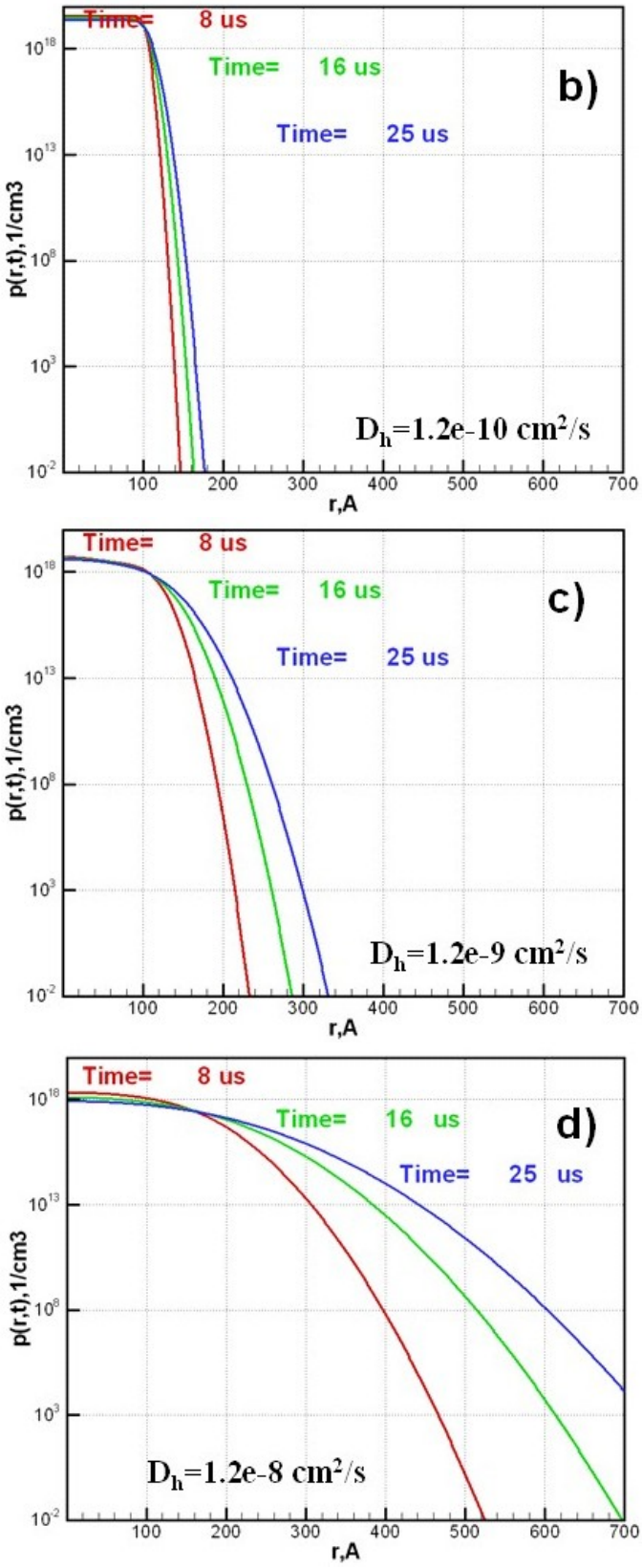

Fig. 3. Results of calculation via the drift-diffusion model in spherical geometry, with the diffusion coefficients shown in the plots: (a) 1.2×10^{-11}, (b) 1.2×10^{-10}, (c) 1.2×10^{-9}, and (d) 1.2×10^{-8} cm^2/s.

Figure 3 shows the hole densities' dependence on time, for an Al_2O_3+ZnO film, for different hole diffusion coefficients.

Figure 4 shows a two-dimensional map illustrating the time/distance dependence of the total electronic charge in the charged volume, obtained for geometry (a), as a result of solution of the equation set (3).

The relaxation times were obtained as a constant of exponential dependencies calculated by the numerical solution of the set (3). They were obtained for various hole diffusion coefficients as shown in Fig. 5: (a) 1.2×10^{-8} cm^2/s; (b) 1.2×10^{-10} cm^2/s; and (c) 1.2×10^{-11} cm^2/s.

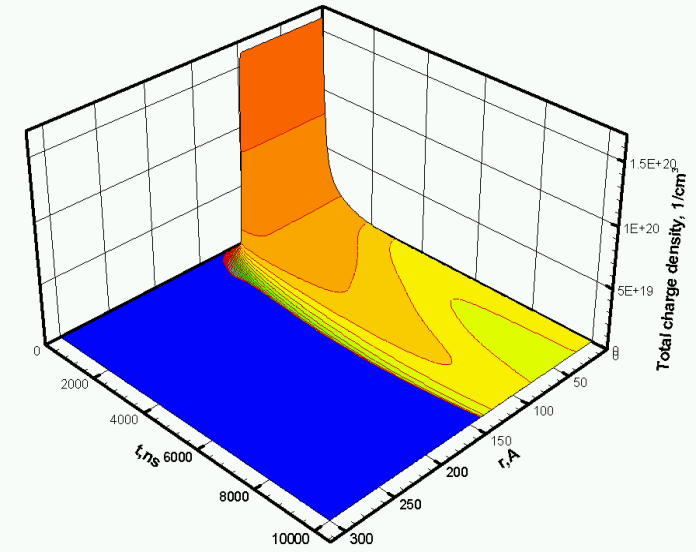

Fig. 4. Results of calculation showing the total charge dependence on the radial distance and time for spherical geometry.

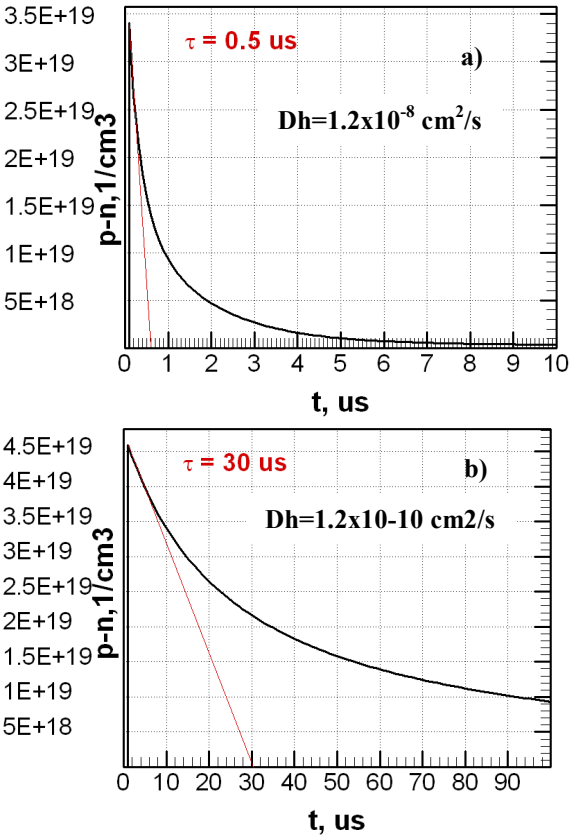

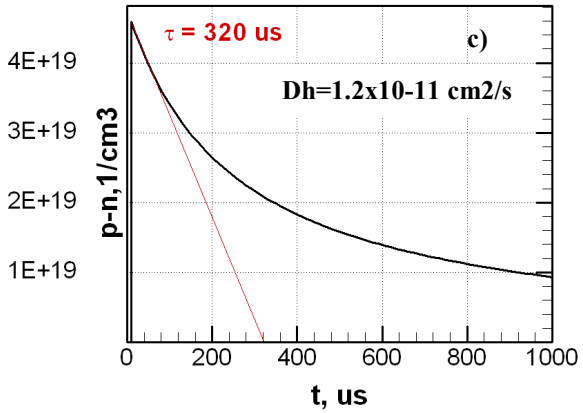

Fig. 5. Calculated charge depending exponentially on time that defines the relaxation times. The hole diffusion coefficient is used a parameter of calculations: (a) $D_h = 1.2\times10^{-8}$ cm^2/s, $\tau = 0.5$ μs; (b) $D_h = 1.2\times10^{-10}$ cm^2/s, $\tau = 30$ μs; (c) $D_h = 1.2\times10^{-11}$ cm^2/s, $\tau = 320$ μs.

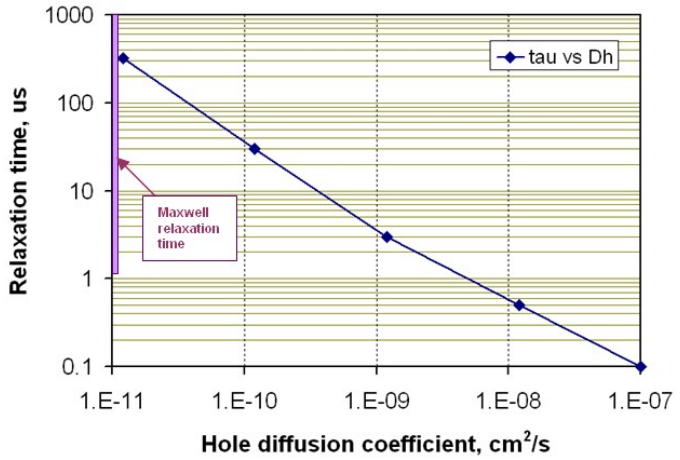

Fig. 6. Calculated dependence of the relaxation time on the hole diffusion coefficients compared with the Maxwell relaxation time shown as a vertical bar on the y-axis.

Figure 6 shows our predictions for the relaxation time depending on the diffusion coefficients of holes. For comparison, the Maxwell relaxation time is given as a vertical bar on the y-axis.

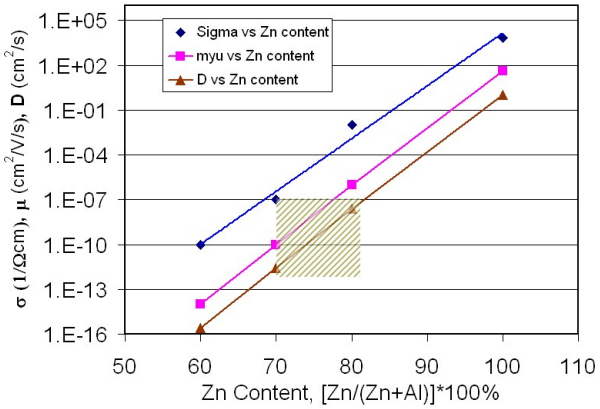

Fig. 7. Proposed materials constants: conductivity, mobility, and diffusion constants obtained as results of calculations of set (3), for an Al_2O_3+ZnO mixture for various zinc contents. The recommended values are shown as the dashed square.

The calculated results in Fig. 7 were compared to the results of a simple Maxwell relaxation time model and with the circuit charge relaxation model developed for the MCP device [10]. A pump-probe experiment discussed in [11] can measure the charge relaxation time and of demonstrating gain depletion. It is based on the attenuation of pulses travelling along a microwave strip line on an MCP beyond that due to normal resistive losses [12].

III. Numerical Model of Saturation Effect

As was shown by A. Guest [13], the longitudinal current distribution in the pore has an exponential dependence. Thus, a huge number of secondary electrons are extracted from the end of the pore for short input pulse and high gain, and a positive charge is induced on the pore surface, thereby suppressing further secondary emission. The current from an external source cannot immediately compensate for the induced charge because of the finite resistance of the secondary emitter material. The saturation effect can be mitigated by making a double-layer cover on the pore surface: a high-conductivity layer below and a high-emission layer on top.

Different models of the saturation effect in an MCP have been suggested in the literature [14–18]. All of them include some coefficients to fit the gain vs. voltage dependence to the experimental data. A. Berkin and V. Vasil'ev give an analytical solution for the pulse [19] and DC [20] work regimes, which include the easily measured parameters only for the electric field

$$E_z(z,t) = E_{0z} h_E(z,t), \tag{4}$$

and gain

$$M(z,t) = M_0 \frac{h_E(z,t)}{1-\left[h_E(z,t_p)-1\right]\exp\left(\dfrac{t_p - T}{\tau}\right)}. \tag{5}$$

The shape function is given by the following formulas:

$$h_E(z,t) = \frac{\ln(M_0)}{\left[\ln(M_0) - \ln(1+C(t)) - \ln(1+C(t)M_0)\right]\left[1+C(t)e^{\alpha z}\right]},$$
$$c(t) = \frac{I_0}{I_R}\left(1 - e^{-t/\tau}\right) . \tag{6}$$

Here E_{0z}, and M_0 are the electric field and gain for the nonsaturated mode, respectively; T and t_p are the pulse period and pulse length, respectively; τ is a charge relaxation time; I_0, I_R are the input current and resistance current, respectively; α is the increment of the emission current in nonsaturated pore $I(z)=I_0 \exp(\alpha z)$, z is the axial coordinate; and t is the time.

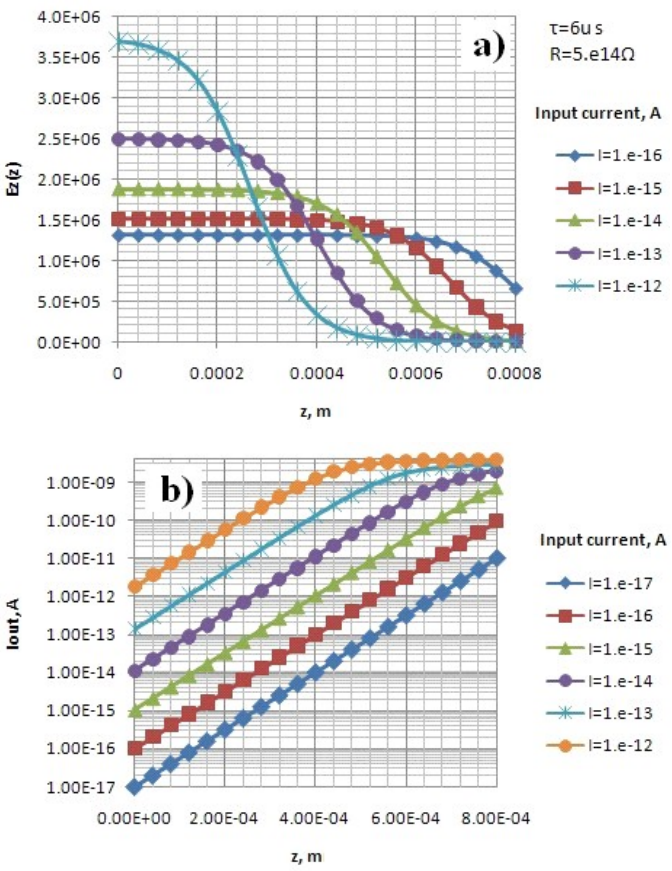

Fig. 8. (a) Field distribution in the channel for different input current; (b) output current distribution vs. input currents.

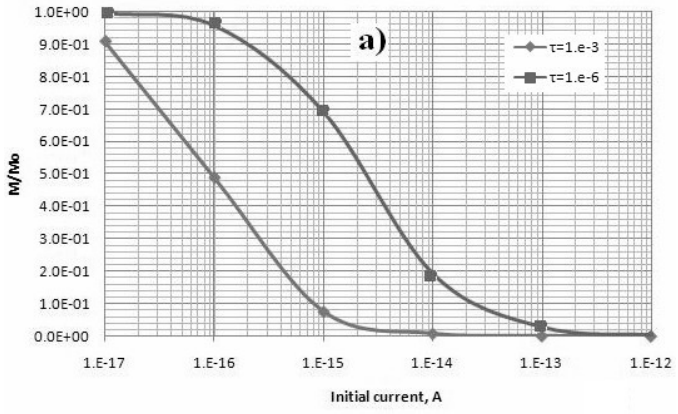

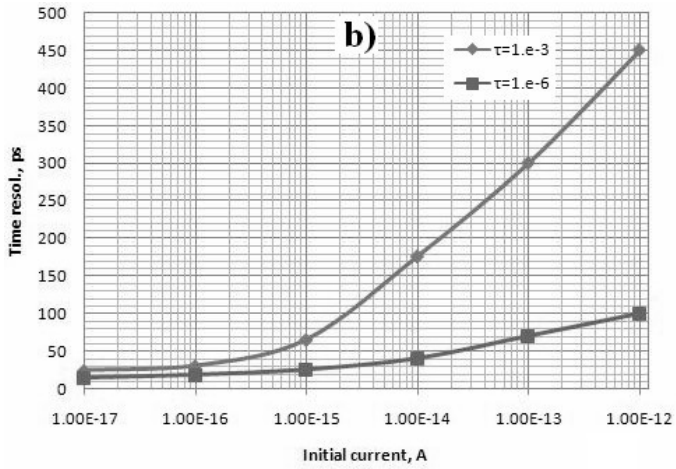

Fig. 9. (a) Gain vs. input current for τ=1 msec and τ=1 μsec; (b) timing resolution vs. input current.

Figures 8 and 9 show the results of our simulations for 20 μm pores of 1.2 mm length. One can see that the saturation effects are negligible for $I_0 < 1\times10^{-15}$ A.

IV. Fringe Field Simulation in 3D

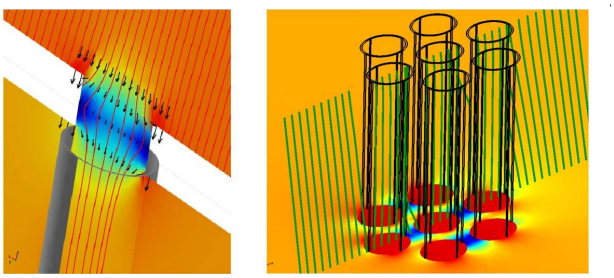

Fig. 10. Lines of electric field in the pores (left) and between them (right).

The simulations show that in a highly conductive environment, the electric field in the pore is directed axially inside the pore, having a gradual turn from the value in the resistive layer near the surface. In a simulation we assume that the relaxation time ε/σ is small for a thin, resistive layer comprising a mixture 30% Al_2O_3 and 70% ZnO.

Figure 10 shows the lines of electric field in 1 and 7 pores with bias angle of 8˚.

Figure 11 demonstrates the edge effect for the electric field at the end of the pore: the angle $\beta = a\tan(E_x / E_z)\cdot 100/\pi$ vs. the z-coordinate of the pore.

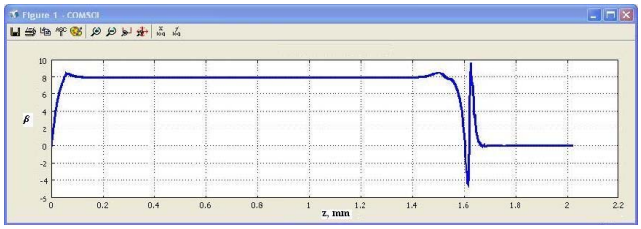

Fig. 11. Edge effect for the electric field.

V. Mitigation of Saturation Effect

Monte Carlo algorithms are commonly used to simulate MCP amplifiers [21]. The effect of interplate gap variation was studied numerically by using the full 3D Monte Carlo simulator code MCS. Figure 12 shows that most of the beam from the first plate is accepted by one pore of the second plate for a gap size of 15 μm. The same initial beam is redistributed for 7 pores of a hexagonal structure in a second MCP for a gap of 100 μm (Fig. 13), which substantially reduces the saturation effect.

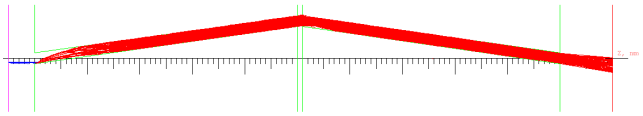

Fig. 12. Small gap: gain M=1.2E6 for τ=1 μs, and M=1.5E5 for τ=1 ms.

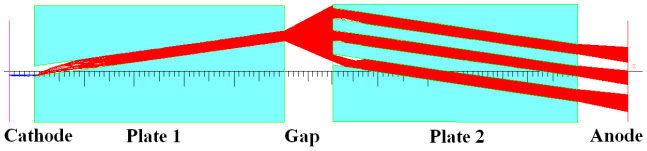

Fig. 13. Large gap: electrons distributed to 7 pores of the second plate. Gain M=3.4E6 for τ=1 μs, and M=1.13E6 for τ=1 ms.

VI. Summary

Relaxation times for a charged spherical and cylindrical areas were calculated by using a diffusion-drift model for an Al_2O_3+ZnO mixture for different material parameters. Recommendations were given for the composition of the emissive/conductive layers that provide acceptable relaxation times and, as a consequence, the gain and the transient times of the MCP device.

Future work includes study of temperature effects that may dramatically change the recommendations as a result of a strong dependency of the materials constants on temperature.

Acknowledgment

This work was supported in part by the Office of Advanced Scientific Computing Research, Office of Science, U.S. Department of Energy, under Contract DE-AC02-06CH11357.

References

[1] J.W. Elam et al., J. of Electrochem. Soc. 150, 6 (2003) G339-G347.
[2] Z. Insepov et al., Phys. Rev. A77 (2008) 062901.
[3] C.F. Herrmann et al., Proc. of SPIE 5715 (2005) 159.
[4] A.K. Jonscher, Principles of semiconductor device operations, Wiley (1960).
[5] A.G. Chynoweth, J. Appl. Phys. 31 (1960) 1161-1165.
[6] A.H. Marshak, Proc. IEEE 72 (1984) 148-164.
[7] R. Van Overstraeten, Solid State Electronics 13 (1970) 583-608.
[8] L.M. Biberman, Proc. IEEE 59, (1972) 555-572.
[9] F. Ruske et al., J. Appl. Phys. 107, (2010) 013708.
[10] A.B. Berkin, V.V. Vasil'yev, Techn. Phys. Lett. 33, (2007) 664-666.
[11] O.L. Landen et al, Proc. SPIE 2002, 2 (1993).
[12] M. Katayama et al., Rev. Sci. Instrum. 62 (1991) 124.
[13] A. J. Guest, Acta Electron. 14, 1 (1971) 79-97.
[14] A. M. Tutikov et al., Sov. J. Opt. Technol. 50, 7 (1991) 392-395.
[15] A. S. Tremsin et al., Nucl. Inst. Meth. A379 (1996) 139-152.
[16] P. M. Shikhalev, Nucl. Inst. Meth. A420 (1999) 202-212.
[17] G. J. Price, G. W. Fraser, Nucl. Inst. Meth A474 (2001) 188-196.
[18] G. W. Fraser et al., IEEE Trans. Nucl. Sci. NS-30, 1 (1983) 455-460.
[19] A. B. Berkin, V. V. Vasil'ev, Zhurn. Techn. Fiziki, 78, 2 (2008) 127-129.
[20] A. B. Berkin, V. V. Vasil'ev, Zhurn. Techn. Fiziki 78, 2 (2008) 130-133.
[21] E. Gatti et al., IEEE Trans. Nucl. Sci. NS-30, 1 (1983) 461-467.